Title

Magnetic domain wall contrast under zero domain contrast conditions in spin polarized low energy electron microscopy

Authors
Zhou, Chao
Chen, Gong
Xu, Jia
et al.

Publication Date
2019-05-01

DOI
10.1016/j.ultramic.2019.02.026

Peer reviewed

Magnetic domain wall contrast under zero domain contrast conditions in Spin Polarized Low Energy Electron Microscopy

Chao Zhou[a], Gong Chen[b,c,*], Jia Xu[a], Jianhui Liang[a], Kai Liu[c,d], Andreas K. Schmid[b,*], Yizheng Wu[a,*]

[a] Department of Physics and State Key Laboratory of Surface Physics, Fudan University, Shanghai 200433, China

[b] NCEM, Molecular Foundry, Lawrence Berkeley National Laboratory, Berkeley, California 94720, USA

[c] Department of Physics, University of California, Davis, California 95616, USA

[d] Physics Department, Georgetown University, Washington, DC 20057, USA.

* Corresponding authors. Email address: gchenncem@gmail.com; akschmid@lbl.gov; wuyizheng@fudan.edu.cn

Abstract

Important applications of spin polarized low energy electron microscopy (SPLEEM) employ this technique's vector imaging capability to resolve domain wall (DW) spin textures. Studying several thin film systems including Co/W(110), Co/Cu(001) and $(Co/Ni)_n$/W(110), we show that an additional contrast can appear at magnetic DWs. By imaging the magnetization as a function of electron landing energy, electron energies are selected at which the magnetic domain contrast vanishes. Surprisingly, under such conditions of zero contrast between magnetic domains, we observe the appearance of magnetic contrast outlining the DWs. This DW contrast does not depend on the DW spin texture. Instead, our measurements show that this DW contrast results from a combination of the energy-dependence of the spin reflectivity asymmetry of the magnetic film, the finite energy width of the spin polarized electron source, and the dispersion of the magnetic prism array that separates the illumination and imaging columns of the instrument. Awareness of this DW contrast mechanism is useful to aid correct interpretation of SPLEEM images.

Keywords

Spin polarized low energy electron microscopy; magnetic domains; magnetic domain walls; magnetic thin films

1. Introduction

Spin polarized low energy electron microscopy (SPLEEM) is a special kind of low energy electron microscopy (LEEM) that uses a spin polarized electron beam to generate magnetic domain images from samples [1,2,3]. Due to its high spatial resolution, SPLEEM provides a valuable means to study magnetic domain structures in surfaces [4] and thin films [5,6,7,8], especially in systems near the spin reorientation transition [9,10,11,12], as well as to study magnetization profiles in magnetic nanoparticles [13,14,15]. The capability to image the orientation of the magnetization vector with high angular resolution makes SPLEEM a particularly useful tool for studying domain wall (DW) spin textures [16,17,18,19]. The energy dependence of electron reflectivity at surfaces is a consequence of the unoccupied electronic structure of the sample, and applying SPLEEM to measure electron reflectivity spectra can be used to determine spin-dependent electronic structures [2,20], as was demonstrated using quantum well states in thin films [21,22,23,24,25].

High lateral resolution in SPLEEM makes it possible to study energy spectra in non-collinear spin textures such as in magnetic DWs. Due to spin-orbit coupling, the electronic structure of non-collinear spin textures can be different from that of collinear ones. Recently, C. Hanneken et al. demonstrated that non-collinear spin textures in magnetic skyrmions can alter the local electronic structure, resulting in a tunneling resistance different from magnetic single domains [26]. More generally, the extent to which the local electronic structure inside magnetic DW may be modulated by the non-collinear spin texture remains an interesting question, and SPLEEM measurements may provide experimental evidence.

Aiming to investigate the influence of non-collinear spin structures on local electronic structure, this study was initiated by measuring energy dependent spectra in several magnetic thin films. In most magnetic film systems, the spin asymmetry signal of the electron reflectivity spectra varies as a function of energy. We found an unusual contrast in magnetic DWs at the electron landing energies where domain contrast from the spin dependence of the electron reflectivity vanishes. This effect is found to be independent of the magnetic materials and substrates. This DW contrast is also independent of the spin rotation chirality inside the DW, but is related to the slope of spin asymmetry spectrum at this energy. Our analysis shows that this effect is caused by the combination of finite energy spread of the electron beam and the dispersion of the magnetic prism array used in the instrument to separate illumination- and imaging columns. Our simulation results are in good agreement with the experimental observations. The discovery of such an instrumental artefact is important for the analysis of magnetic domain structure and is useful to aid correct interpretation of SPLEEM images.

2. Experiments

Our experiments were performed in the SPLEEM systems at the National Center for Electron Microscopy at the Lawrence Berkeley National Laboratory [1]. The SPLEEM measurements were performed on Co/W(110), $(Co/Ni)_n$/W(110) and Co/Cu(001) thin film/multilayer systems. The W(110) substrate was cleaned by cycles of flash heating to 1950 ℃ in 3×10^{-8} Torr O_2 background followed by a final annealing at the same temperature under ultrahigh vacuum [14]. The Cu(001) substrate was cleaned by several cycles of Ar-ion sputtering and annealing to 550 ℃, followed by a final annealing at the same temperature in ultrahigh vacuum [12]. Co and Ni films were deposited at room temperature from electron beam evaporation sources. The film thickness was controlled by monitoring the electron reflectivity oscillations associated with atomic layer-by-layer growth.

All the SPLEEM images were measured at room temperature on the as-grown samples which were also prepared at room temperature. During the SPLEEM measurements, the sample was biased with a start voltage (V_s), which determines the electron landing energy [2]. The magnetic contrast, which strongly depends on the start voltage V_s, is determined by measuring the spin-dependent reflectivity asymmetry A between the spin-polarized beams with opposite polarization. SPLEEM images are then calculated pixel-by-pixel using $A=[I_\uparrow(V_s)-I_\downarrow(V_s)]/[I_\uparrow(V_s)+I_\downarrow(V_s)]$ where $I_\uparrow(V_s)$ and $I_\downarrow(V_s)$ are the electron reflectivities with up and down spin polarization. To enhance image quality, sequences of images are acquired under identical conditions and residual thermal drift is corrected using image cross-correlation software. Averaging such drift-corrected image sequences results in signal-to-noise optimized images. For a particular sample, the magnetic contrast A in a SPLEEM image is known to be proportional to the product of local unit-magnetization vector $\boldsymbol{m}$ and electron beam polarization $\boldsymbol{\sigma}$, i.e. $A(V_s)=c(V_s)\boldsymbol{m}\bullet\boldsymbol{\sigma}$, where the coefficient $c(V_s)$ strongly depends on the start voltage V_s. The magnetic contrast A is zero for nonmagnetic samples ($\boldsymbol{m}$=0) and for magnetic samples with $\boldsymbol{m}$ perpendicular to $\boldsymbol{\sigma}$ ($\boldsymbol{m}\perp\boldsymbol{\sigma}$). On the other hand, the coefficient $c(V_s)$ is related to the electronic band structure of the sample, and could cross zero at certain V_s, in such cases the magnetic contrast A can be zero even for the magnetic sample with $\boldsymbol{\sigma}$ parallel to $\boldsymbol{m}$ ($\boldsymbol{m}//\boldsymbol{\sigma}$) [18-22]. During the SPLEEM measurements, we first precisely adjusted the spin orientation $\boldsymbol{\sigma}$ to be aligned parallel to the magnetization orientation $\boldsymbol{m}$ in imaged domains, then we measured the energy-dependent asymmetry spectra $A(V_s)$ of the same magnetic domains. From the measured $A(V_s)$ spectra, we determined values of V_{s0} with zero domain contrast $A(V_{s0})$. If the electronic structure indeed is modulated by non-collinear spin structures, then it is expected that the $A(V_s)$ spectra inside the DW would be different from that in the collinearly magnetized domains. Specifically, one would expect that the zero-contrast conditions $A(V_{s0})$ might be shifted in energy, so that at start voltage V_{s0} with zero contrast in the domains it is possible to observe the magnetic contrast inside the DW. In search of such band structure effects we carefully investigated the magnetic contrast $A(V_s)$ in DWs – compared to domains, as a function of V_s.

3. Experimental results

We first present the typical measurements from a 4 monolayer (ML) Co film grown on W(110) substrate, as shown in Figure 1. Co/W(110) films have strong in-plane uniaxial magnetic anisotropy [27], consequently there are only two types of magnetic domains separated by 180-degree DWs. The LEEM image in the inset of Fig. 1(a) shows clear atomic steps, which demonstrates high quality of this film. Moreover, during the Co film growth, the electron reflectivity shows clear intensity oscillation [24], which supports the layer-by-layer growth of Co film.

The measured reflectivity spectrum $R(V_s)$ and spin asymmetry spectrum $A(V_s)$ with

$\boldsymbol{m}//\boldsymbol{\sigma}$ both exhibit clear oscillations due to the electron Fabry-Pérot interference in the Co film [18-22], as shown in Figs. 1(a) and 1(b). The asymmetry spectrum $A(V_s)$ also shows clear sign reversal, which causes the domain contrast to alternate as a function of V_s. For example, the SPLEEM domain images acquired with V_s=4.5 V and 6.2 V have opposite contrast, although the domain contrast for V_s=4.5 V is smaller than that for V_s=6.2 V, as shown in Fig. 1(c) and 1(d). The $A(V_s)$ spectrum in Fig. 1(b) shows zero asymmetry signal at V_{s0}=4.9 V and 6.9 V, which indicates that at these electron energies no contrast should be visible between the domains even when the spin polarization is parallel to the magnetization. Moreover, magnetic contrast within DWs should vanish under these imaging conditions, both because of the vanishing asymmetry signal and, in addition, because orthogonal alignment between the magnetization $\boldsymbol{m}$ and the beam polarization $\boldsymbol{\sigma}$ within the DWs cause the asymmetry $A(V_s)=c(V_s)\boldsymbol{m}\cdot\boldsymbol{\sigma}$ to vanish at all energies. However, SPLEEM measurements at V_s=4.9 V and 6.9 V show a surprising result: we find that unusual bright or dark contrast appears along DWs, as shown in Figs. 1(e) and 1(f). For V_s=4.9 V, the left DW in Fig. 1(e) has dark contrast, and the right DW has bright contrast. For V_s=6.9 V, this contrast in the two DWs is reversed. The strength of this DW contrast at these two energies can be quantified, as shown in the line profiles plotted in Fig. 1(g).

In SPLEEM experiments the spin orientation of the incident electron beam can be adjusted to point along any direction (this enables the technique's vector imaging capability to resolve DW spin textures [16,17,18,19]). We adjusted the incident electron spin perpendicular to the magnetization in the domain, i.e. $\boldsymbol{m}\perp\boldsymbol{\sigma}$: imaging with this spin alignment confirms that the DW spin texture in the Co/W(110) system is Néel-type [28] with the magnetization inside the DWs lying in the film plane. Figure 2(a) and 2(b) show such SPLEEM images, measured at V_s=4.5 V and 6.2 V, respectively. These two images show DWs with opposite magnetic contrasts as a result of the sign reversal of the asymmetry $A(V_s)$ between these energies, see Fig. 1(b). The 180°DWs appear in black or white contrast, depending on the rotation sense of the in-plane spin texture within the DW. However, the new DW contrast that we observe at electron energies V_s=4.9 V and 6.9 V, as shown in Fig. 1(e) and 1(f), appears in a homogeneous black or white contrast, independent of the rotation sense of the DW spin texture. Moreover, we performed SPLEEM measurements at V_s=4.9 V and 6.9 V with $\boldsymbol{m}\perp\boldsymbol{\sigma}$. Although $c(V_s)$ is zero at V_s=4.9 V and 6.9 V, a new kind of DW contrast is now observed within the DWs [Figs. 2(c) and 2(d)]. Different from the uniform contrast in the case of $\boldsymbol{\sigma}||\boldsymbol{m}$, as shown in Fig. 1, in the case of $\boldsymbol{m}\perp\boldsymbol{\sigma}$ alternating black and white contrast now traces the DWs. This DW contrast also reverses sign for V_s=4.9 V versus 6.9 V respectively. The alternating contrast across the DWs can be quantified by line profiles as shown in Fig. 2(e). It should be noted that the DW contrast, as shown in Fig. 2(c) and 2(d), also reverses sign as a function of the rotation sense of the in-plane spin texture within the DW.

To understand this unusual DW contrast, we focus on the observation that in the condition $\boldsymbol{m}//\boldsymbol{\sigma}$ this contrast does not depend on the rotation sense of the magnetization within the DW, see SPLEEM images in Figs. 1(e) and 1(f). This suggests that the contrast may be related to the DW magnetization component orthogonal to the electron spin, or it may be related to the magnetization gradient across the DW. In order to investigate the relation between the observed DW contrast and the magnetization component orthogonal to the electron beam spin polarization, we performed the experiments on the Co(15 ML)/Cu(001) system. This system has an in-plane four-fold magnetic anisotropy [29], thus it contains 90° DWs. Fig. 3(a) and 3(b) show the reflectivity spectrum $R(V_s)$ and the spin asymmetry spectrum $A(V_s)$ respectively. A sign reversal of the asymmetry occurs at V_{s0}~7.8 V. Although the Co/Cu(001) system has four-fold symmetry, an additional two-fold symmetry is due to the small miscut of the substrate, which distinguishes the step array in the LEEM image shown in Fig. 3(a) inset. Due to this step-induced two-fold symmetry, 180^o DWs dominate the magnetic domain structure in the as-grown sample [30]. SPLEEM image at V_s~10.5 V with the spin polarization aligned along Cu[110] (Fig. 3d), clearly shows grey areas between the white and dark regions. When the spin polarization is rotated by 90°, i.e. spin polarization aligned along Cu[$1\bar{1}0$] (Fig. 3e), the areas that are grey in Fig. 3(d) now show strong white and black contrast in Fig. 3(e). Taken together, the SPLEEM images in Figs. 3(d,e) establish magnetization directions as indicated by the arrows in Fig. 3(d), i.e. the smaller domain near the middle of the images is magnetized along Cu[$1\bar{1}0$], and it is separated by 90° DWs from the large domains magnetized along Cu[110]. As in the case of Co/W(110) described above, we find again the similar DW contrast in SPLEEM images of Co/Cu(100) acquired at electron energy with zero spin contrast, i.e. at V_s~7.8 V. For electron beam spin polarization aligned along Cu[110], we observe the DW contrast at the 180° DWs, as indicated by the line profiles A and B in Fig. 3(c). A similar contrast can also be observed at 90° DWs, see Fig. 3(f), although it is weaker than that at 180° DWs; the spin contrast at 90° DWs is more clearly confirmed by the line profile C shown in Fig. 3(c). No additional contrast is observed within the small domain where the magnetization is perpendicular to the spin polarization in Fig. 3(f). This indicates that the usual DW contrast in Fig. 1 and Fig. 3 is not related to the orthogonal relation between the spin polarization $\boldsymbol{\sigma}$ and the magnetization $\boldsymbol{m}$ within DWs.

We now consider the possibility that the unusual DW contrast may be related to the magnetization gradient across the DWs. An unconventional gradient effect in magnetic DW imaging has also been reported in magneto-optic microscopy studies [31,32]. R. Schafer and A. Hubert first reported this new magneto-optic effect related to non-uniform magnetization on the surface of a ferromagnet, and found an unexpected alternating domain boundary contrast not related to the internal structure of the DWs [33]. This magneto-optic gradient effect has been explained by diffraction theory [34,35]. One may conjecture that the unconventional SPLEEM DW contrast is proportional to the magnetization gradient, i.e. $\propto \nabla(\mathbf{m} \cdot \boldsymbol{\sigma})$. This would be consistent with the fact that the unconventional DW contrast is independent of the magnetization rotation sense inside DWs in Fig. 1 and Fig. 3, and it is consistent with the observed opposite contrast in the neighboring DWs, which have opposite magnetization gradient. Magnetization gradient dependent contrast can also explain the alternating black and white DW contrast in images acquired with the spin polarization perpendicular to the magnetization in the wall.

The proposed link with the DW magnetization gradient suggests that investigating the dependence of the unconventional DW contrast on varying DW orientation may yield key clues. So, we further studied the unconventional DW contrast in $(Co/Ni)_n$ multilayers grown on W(110). This system contains many small domains with domain sizes comparable to the SPLEEM field of view (10 μm in this work), which allows us to study the dependence of the DW contrast on continuously varying DW orientation [8,13]. Moreover, in the $(Co/Ni)_n$/W(110) system, the in-plane easy axis can be tuned from [001] to $[1\bar{1}0]$ by adjusting the relative thickness ratio of Co and Ni layers [8].

Figure 4 shows SPLEEM images of $Co(2)/[Ni(2)/Co(1)]_2$/W(110) and $[Co(1)/Ni(3)]_2$/W(110) with the easy axis along [001] and $[1\bar{1}0]$ respectively (numbers inside round brackets indicate the corresponding film thickness in units of atomic monolayer). Figs. 4(a) and 4(b) show the corresponding asymmetry spectra with multiple sign reversals. Fig. 4(c) shows a SPLEEM image of $Co(2)/[Ni(2)/Co(1)]_2$/W(110), acquired at V_{s0}=5.25 V, where $A(V_{s0})=0$ and thus no domain contrast is observed. Similarly, Fig. 4(d) shows a SPLEEM image of $[Co(1)/Ni(3)]_2$/W(110) with zero domain contrast at V_{s0} =5.35 V. These images, panels 4(c) and 4(d), provide a clue to the origin of the observed DW contrast: note that in Fig. 4(c) the DW contrast is white in the left DW and black in the right DW, while in Fig. 4(d) the DW contrast is reversed. Noting the opposite slopes of the corresponding $A(V_s)$ curves in Fig. 4(a) and 4(b), as indicated by the red arrows, this suggests a possible relationship between the observed new DW contrast and the slope of the asymmetry curves $A(V_s)$. An additional clue is the observation of vanishing DW contrast within DW sections aligned approximately horizontally in Fig. 4(c) and 4(d), as highlighted by the red oval surrounding the bottom horizontal DW sections. On the top horizontal DW sections, the DW contrast gradually changes its sign, but the contrast vanishing behaviour is less obvious, since the DW orientation there changes more rapidly. We analysed DW contrast visibility quantitatively, in terms of asymmetry A, as a function of the wall orientation angle θ_{DW}. The $A(\theta_{DW})$ curves of both samples, reproduced in Figs. 4(e) and 4(f), can be well described by the relation $A_0\sin(\theta_{DW}-\theta_0)$, where A_0 is the maximal value of this DW contrast and θ_0 as the offset angle with the zero contrast. The best-fit value of θ_0 in both measurements is 7° and 27° respectively. Although the in-plane easy magnetization axis in $Co(2)/[Ni(2)/Co(1)]_2$/W(110) is rotated by 90°

compared to $[Co(1)/Ni(3)]_2/W(110)$, in both samples zero contrast of the DWs occurs when the DWs are nearly parallel to the x-axis. This indicates that the observed DW contrast is independent of both the magnetization orientation and the crystal axis orientation. If this DW contrast were to originate from the intrinsic magnetic properties of the system, then it would be plausible to expect that the DW contrast should change when the magnetic easy axis is rotated, i.e., the zero-contrast angle θ_0 should be offset by 90° between $Co(2)/[Ni(2)/Co(1)]_2/W(110)$ and $[Co(1)/Ni(3)]_2/W(110)$ as a result of orthogonal magnetization orientations in the two systems. However, the experimental values of θ_0 in the two systems are very close, which indicates that the observed DW contrast may have an extrinsic origin related to the SPLEEM instrumentation.

Searching for a possible extrinsic origin of the unusual DW contrast, we carefully explored the dependence of this DW contrast on changing the electron energy to values V_s slightly different from V_{s0}. In Figs. 5(a) and 5(c), SPLEEM images of the $Co(2)/[Ni(2)/Co(1)]_2/W(110)$ sample at V_s=5.2 V and 5.3 V, respectively, clearly show the magnetic domains with opposite contrast. In addition the image at V_{s0}=5.25 V shows the DW contrast. Careful inspection reveals that the contrast at the left domain boundary in both Figs. 5(a) and 5(c) is slightly brighter than that at the right domain boundary. This contrast difference can be clearly identified in the line profiles shown in Fig. 5(e), where line profiles of the SPLEEM images at 5.2 V and 5.3 V show small peaks at left DW and small dips at right DW, as indicated by arrows in Fig. 5(e). Inspecting reversed domain contrast above and below V_{s0}, in combination with non-reversing contrast peaks at the domain boundaries, stimulated our hunch to consider the image formed in a pixel-by-pixel sum of the two SPLEEM images acquired at 5.2 V and 5.3 V, just below and above the zero-asymmetry electron energy. The result of summing the images is shown in Fig. 5(d), which looks strikingly similar to the SPLEEM image measured at 5.25 V with zero domain contrast, shown in Fig. 5(c).

Similar image summation operation can also be done in the SPLEEM measurements of the Co/W(110) system. As shown in Fig. 1, the domain contrast is maximum at 4.5V and 7.5 V, but minimum at 6.2V. If the SPLEEM images acquired at 4.5V and 6.2 V are added together, the resultant image reproduced in Fig. 6(a) shows contrast along

DWs that appears very similar to the DW contrast observed in the SPLEEM image measured at 4.9 V [Fig. 1(e)]. Here in order to remove the unbalanced domain contrast at 4.5 V and 7.5 V, the domain contrast in the 4.5 V and 7.5 V images was normalized to 1 before the summation operation. Likewise, summation of images acquired at 6.2 V and 7.5 V results in the image shown in Fig. 6(b), which is similar to the SPLEEM image acquired at 6.9 V [Fig. 1(f)], and reproduces the observed DW contrast. This image summing operation can also be done for images recorded with the electron polarization perpendicular to the domain magnetization, $\boldsymbol{m}\perp\boldsymbol{\sigma}$, and the resultant summed images shown in Figs. 6(c) and 6(d) are very similar to the SPLEEM images shown in Figs. 2(c) and 2(d), reproducing the alternating black and white contrast across the DWs.

4. Discussions

Figures 1-4 show that the observed DW contrast is independent of the magnetization orientation within the domains, and independent of the rotation sense of the DW spin texture, which suggests that this DW contrast does not originate from the magnetic properties. Moreover, the summation operations shown in Figs. 5 and 6 can reproduce the DW contrast observed in the SPLEEM images measured at V_{s0}. This observation suggests a possible extrinsic origin related to the SPLEEM instrumentation, as we discuss below.

As shown by the reflectivity spectra in Fig. 1(a) and Fig. 3(a), the electron reflectivity quickly drops for the electron energy above the workfunction within a certain energy range, and the energy width of this dropoff corresponds to the energy width of incident electron beam. The energy width of the spin polarized beam used in these measurements is estimated to be ~0.3 eV, this energy distribution is sketched schematically in Fig. 7(a). While the SPLEEM measurement is performed at V_{s0}, half of the electrons with lower energy will produce an image with positive domain contrast, while the other half of the electrons with higher energy will produce an image with the opposite domain contrast, as sketched in Fig. 7(b), left- and middle panels. If these two images, acquired with energy below and above V_{s0}, are slightly displaced from each other, then contrast can appear at domain walls. SPLEEM images correspond to averages of all the electrons: as shown in the right panel of Fig. 7(b), representing the pixel-by-pixel average of the left and middle panels, under conditions of energy dependent image shift the magnetic domain contrast vanishes in all image areas, except in close proximity to the DWs. Due to the displacement between images resulting from different tails in the beam energy distribution, bright and dark bands outline the DW, and this effect vanishes only in sections where the DW is oriented parallel to the horizontal image shift. The DW contrast at V_{s0} for the incident electron spin perpendicular to the domain magnetization ($\boldsymbol{m}\perp\boldsymbol{\sigma}$) shown in Fig. 2 can also be explained by the energy-dependent image shifting effect. Under this measurement condition, only the DWs have the magnetic contrast, and the energy-dependent image shifting around V_{s0} can result in the oscillating white and black contrast cross the DWs.

In this picture, it is clear that, if the asymmetry spectrum has the opposite slope as that shown in Fig. 7(a), then the domain contrast should also be opposite to that shown in Fig. 7(b). This is consistent with the observation of the opposite DW contrast at 4.9 V and 6.9 V in the Co/W(110) system (Fig. 1), which can be attributed to the opposite slope at these two energies in the asymmetry spectrum. Likewise, in Fig. 4(c) and 4(d) the reversed DW contrast can be attributed to the opposite slope in the corresponding asymmetry spectra shown in Fig. 4(a) and 4(b).

Based on this picture, we can quantitatively reproduce the observed DW contrast through simulations. We consider a circular domain with the diameter of 3.6 μm, surrounded by a DW with a width of 150 nm, similar to magnetic domain structures imaged in Fig. 1. As shown in Fig. 7(a), we model the incident electron beam as having a Gaussian energy distribution with the half-peak width of ΔV=0.3 V. With approximately linear dependence of the asymmetry on the electron energy (4.9% per electron volts derived from the asymmetry spectrum in Fig. 1), we can compute a weighted sum of all domain images across this energy range, accounting for image weight following the Gaussian distribution. To include the energy-dependent image shift, we assumed that images are shifted along the horizontal direction by 430 nm/V. The resulting simulated image shows bright contrast in the left DW and dark contrast in the right DW. The amplitude of the simulated DW contrast is about 0.49% at V_{s0}. Considering that the measured DW contrast is ~0.29% at 4.9 V and ~0.50% at 6.9 V, our simulation quantitatively reproduces the measured DW contrast, which further supports our interpretation that the observed DW contrast at V_{s0} is likely due to beam energy spread combined with energy-dependent image shift.

The suggested energy-dependent image shift can be measured by modulating the electron energy in the SPLEEM. To this end a voltage source was connected to the cathode in the SPLEEM electron gun to measure how much the image position can be influenced by modulating the electron beam energy without changing the imaging condition in the imaging column. This experiment was performed on a high-contrast sample of Pd(0.15ML)/Ru(0001). Fig. 7(c) shows that the LEEM image of this Pd/Ru surface contains Pd nano-dots with bright contrast [36], and Fig. 7(d) shows that the image is shifted by ~150 nm to the left, as indicated by the red outlines in Fig. 7(c) and 7(d), when the cathode potential is raised by 0.35 V. For reference, the orange circle highlights a permanent defect on the phosphor screen. Thus the magnitude of the energy-dependent image shift is ~430 nm/V, as used in our simulation described above. The direction of this observed energy dependent image shift coincides with the beam-deflection plane of the magnetic beam separation prism, approximately 10° with respect to the image horizontal direction of our CCD camera. As a final test, we reproduced the observed DW contrast by modulating the electron beam energy by applying a 1000 Hz square wave voltage to the cathode. SPLEEM image acquisition time is usually in the range of second, thus the electron energy modulation at much higher frequency essentially simulates a controlled increase of the energy width of the beam. Figs. 7(e) and 7(f) show the measured DW images at V_{s0}~4.9 V under energy modulation with the amplitudes of 0.2 V and 0.4 V respectively. A clearer DW contrast can be identified in Fig. 7(f) for the higher amplitude of electron energy modulation, showing that increased beam energy broadening induces stronger DW contrast at V_{s0} where the contrast between homogeneously magnetized domains vanishes.

5. Conclusion

In summary, we observed unusual DW contrast in SPLEEM measurement on different magnetic films. This DW contrast appears only at electron energy where the contrast between homogeneously magnetized domains vanishes. This contrast is related to the slope of the spin asymmetry spectrum at such energies, and is independent of the spin rotation sense inside the DWs. Our control experiments indicate that this new DW contrast is attributed to the energy width of the incident electron beam and energy-dependent image shifts resulting from the dispersive properties of the electron optics used in the SPLEEM instrument. Although the energy spread of the electron beam can be neglected in the interpretation of most SPLEEM measurements, dependence of the contrast observed here on the slope of spin asymmetry spectra suggests that the beam energy broadening may introduce effects that must be taken into account in some circumstances. This DW contrast might not play a significant role in the SPLEEM images acquired at beam energy with strong domain contrast, but it may influence spin texture measurements in experiments investigating conditions with weak spin contrast. The observed DW contrast is proportional to the energy-dependent slope of the spin asymmetry spectrum, thus it doesn't influence the interpretation of earlier DW studies using SPLEEM with the electron energy at the maxim domain contrast. However, our work suggests that interpretations of complex SPLEEM images with non-collinear domain structures may benefit from careful analysis.

Acknowledgements

The work at Fudan University was supported by the National Key Basic Research Program of China (Grant No. 2015CB921401), National Key Research and Development Program of China (Grant No. 2016YFA0300703), National Natural Science Foundation of China (Grants No. 11474066, No. 11734006 and No. 11434003), and the Program of Shanghai Academic Research Leader (No. 17XD1400400). Work at the Molecular Foundry was supported by the Office of Science, Office of Basic Energy Sciences, of the US Department of Energy under contract no. DE-AC02-05CH11231. Work at UCD was supported by the UC Office of the President Multicampus Research Programs and Initiatives MRP-17-454963 (G.C.) and NSF

392 DMR-1610060 (K.L.).

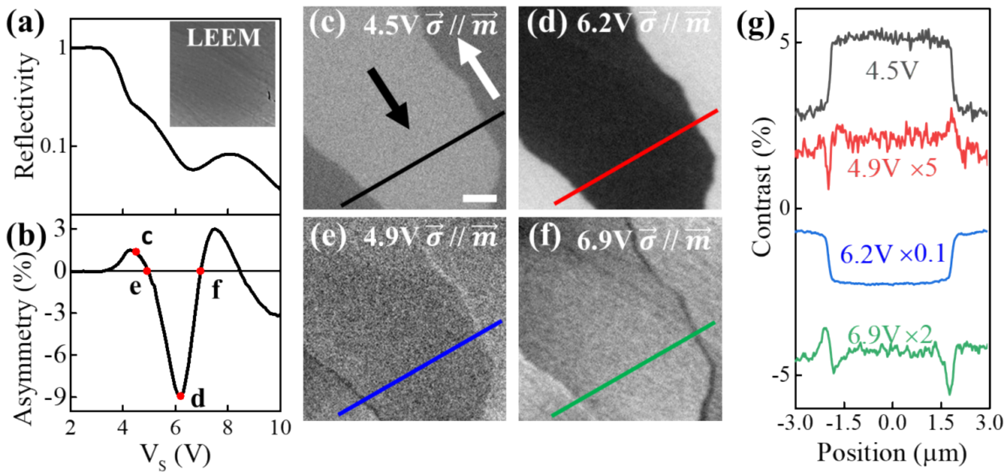

Fig. 1 (a)-(b) Reflectivity and spin asymmetry spectra of Co(4ML)/W(110). Inset is a LEEM image of this sample taken with V_S=5 V. The red dots in (b) indicate the electron energies Vs used for the SPLEEM images in (c-f). (c)-(f) SPLEEM images of the same position at different V_S (4.5 V, 4.9 V, 6.2 V, 6.9 V) for the electron polarization $\vec{\boldsymbol{\sigma}}$ parallel to the magnetization $\vec{\boldsymbol{m}}$ in the domains ($\boldsymbol{m}//\boldsymbol{\sigma}$). The scale bar in (c) is 1 μm. (g) Line profiles from (c)-(f) in the area marked with the lines in corresponding color..

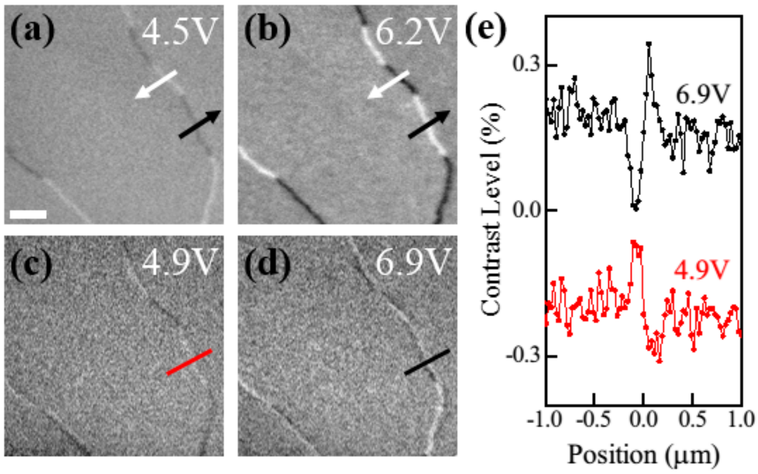

Fig. 2 (a)-(d) SPLEEM image of the same position as Fig. 1 at different V_S (4.5 V, 4.9 V, 6.2 V, 6.9 V) with electron polarization $\vec{\boldsymbol{\sigma}}$ perpendicular to the magnetization $\vec{\boldsymbol{m}}$ in the domains ($\boldsymbol{m}\perp\boldsymbol{\sigma}$). The scale bar in (a) is 1 μm. (e) Line profiles from the corresponding-color lines cross the DWs in (c) and (d), which demonstrate the alternating white and dark contrast across the DWs.

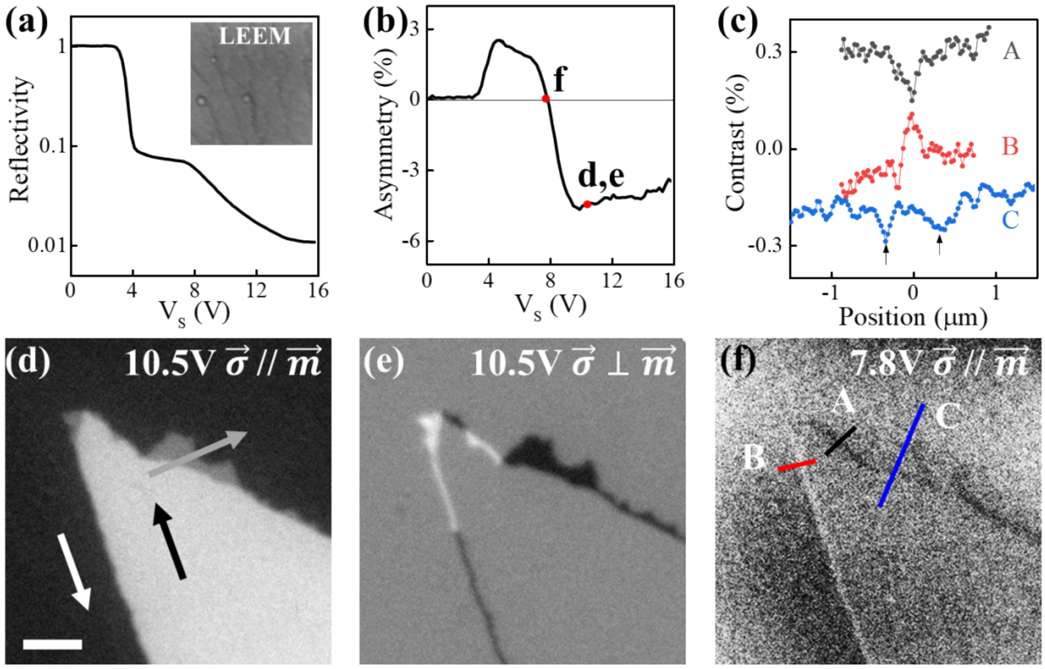

Fig. 3 (a) Reflectivity spectrum and (b) Spin asymmetry spectrum of Co(15 ML)/Cu(001). Inset in (a) is the LEEM image of this sample with V_S=5 V. The red dots in (b) indicate the electron energies Vs used for the SPLEEM images in (d-f). (c) Line profiles from the marked positions in (f). (d)-(f) SPLEEM images of the same position with different combinations of V_S and the electron polarization direction: (d) V_S=10.5 V, $\vec{\boldsymbol{\sigma}}$ // $\vec{\boldsymbol{m}}$, (e) V_S=10.5 V, $\vec{\boldsymbol{\sigma}} \perp \vec{\boldsymbol{m}}$, and (f) V_S=7.8 V, $\vec{\boldsymbol{\sigma}}$ // $\vec{\boldsymbol{m}}$. The scale bar in (d) is 1 μm. Arrows in (d) indicate magnetization directions.

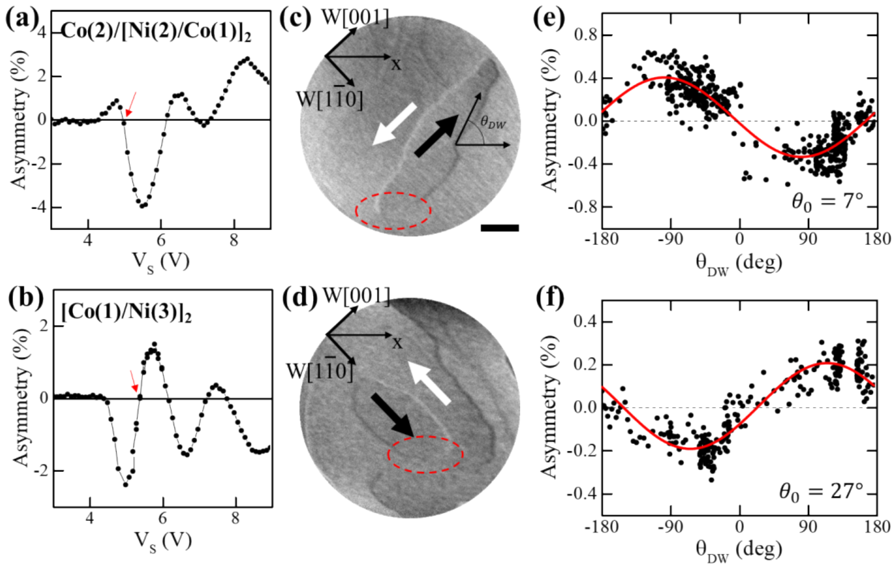

Fig. 4 Asymmetry spectra of (a) Co(2)/[Ni(2)/Co(1)]$_2$/W(110) and (b) [Co[1]/Ni(3)]$_2$/W(110). SPLEEM images in (c) of Co(2)/[Ni(2)/Co(1)]$_2$/W(110) with V_S=5.25 V, and (d) of [Co[1]/Ni(3)]$_2$/W(110) with V_S=5.34 V. The scale bar in (c) is 2 μm. The red circles in (c) and (d) mark the DW section where the unusual DW contrast vanishes. (e)-(f) Contrast inside the DWs in (c) and (d) as a function of DW orientation θ_{DW}, as defined in (c). The red lines at fitting curves with the function $A_0\sin(\theta_{DW}-\theta_0)$. The best-fit values of θ_0 are indicated inside the figures.

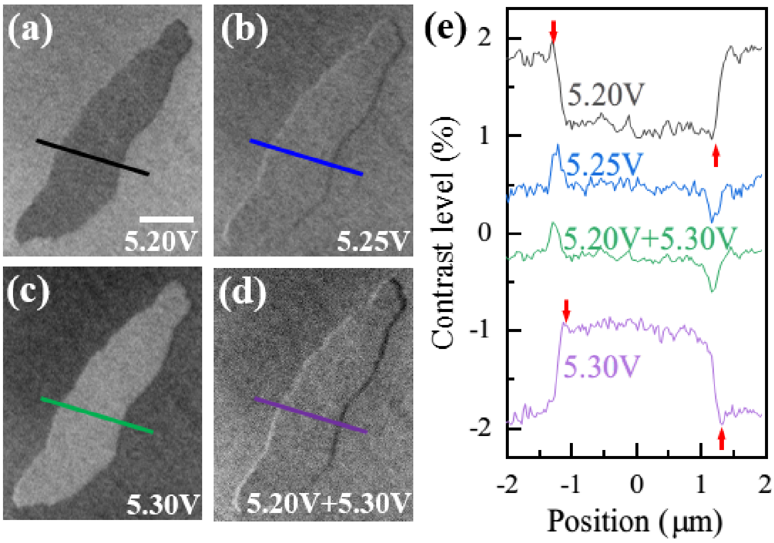

Fig. 5 (a)-(c) SPLEEM images of Co(2)/[Ni(2)/Co(1)]$_2$/W(110) with V_s of 5.2 V, 5.25 V and 5.3 V respectively. (d) Pixel-by-pixel averaged image of the SPLEEM images at 5.2 V in (a) and 5.3 V in (c), which is similar to the measured SPLEEM image at 5.25 V in (b). The scale bar in (a) is 2 μm. (e) Line profiles across the corresponding-color lines in (a)-(d). Red arrows indicate small peaks and dips in the contrast, see main text.

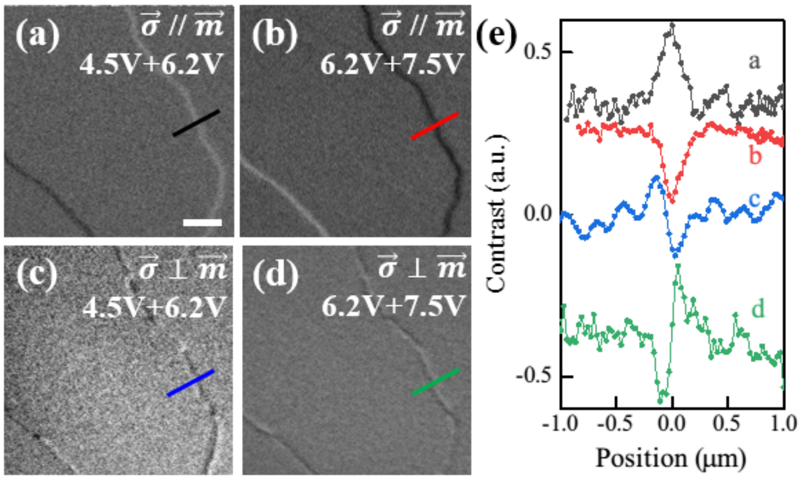

Fig. 6 (a)-(d) Averaged SPLEEM images of Co(4 ML)/W(110). The values of Vs and the spin polarization orientation are marked in the figures. The scale bar in (a) is 1 μm. (e) Line profiles from the corresponding-color lines in (a)-(d).

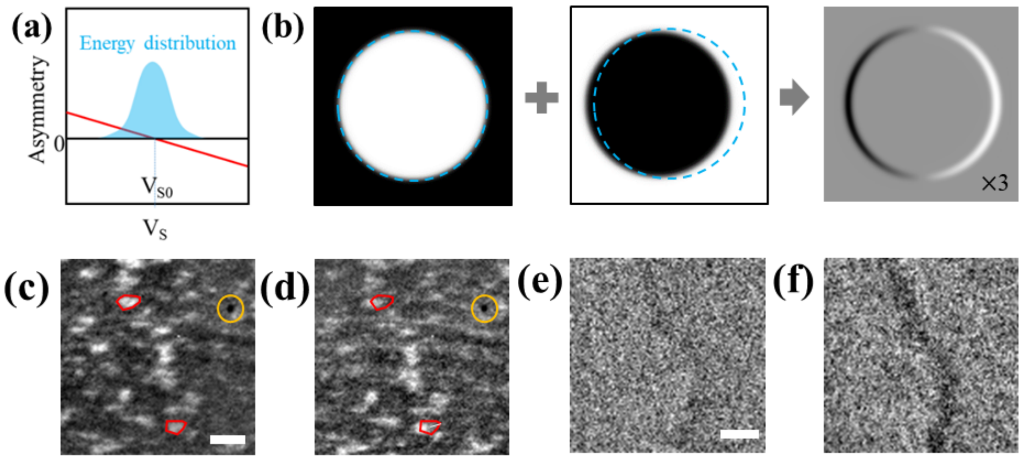

Fig. 7 . (a) Schematic drawing of spin asymmetry spectrum (red curve) near V_{s0}, and the distribution of electron energy (blue area). (b) Schematic drawing of the contrast simulation of a circular magnetic domain, including the energy dependent image displacement due to dispersion in the beam separation prism array in our SPLEEM instrument. Image at higher electron energy (middle) is displaced slightly to the left with respect to the image at lower energy (left). Averaging these two images (right) results significant contrast on domain boundary, and the simulated DW contrast was enhanced by a factor of 3, which means the simulated DW contrast is about one third of the domain contrast at V_{s0}±0.3 V (see main text). (c) LEEM image of Pd(0.15 ML)/Ru(0001), bright areas are Pd islands, dark areas are bare Ru surface. (d) LEEM image obtained with electron gun cathode potential raised by additional 0.35 V, imaging conditions otherwise identical to (c). Red outlines highlight the image shift in panel **c** and **d**, for clarity orange circle highlight a defect on screen which does not move. (e) and (f), SPLEEM images of Co(4 ML)/W(110) at 4.9 V while applying a 1000 Hz square wave voltage the cathode with the amplitude of (e) 0.2 V and (f) 0.4 V respectively. Scale bars in (c) and (e) are 500 nm.

461 **References**

---

1 N. Rougemaille and A. K. Schmid, Magnetic imaging with spin-polarized low-energy electron microscopy. Eur. Phys. J. Appl. Phys. 50 (2010) 20101.
2 E. Bauer, Spin-polarized low energy electron microscopy, in: H. Kronmueller, S. Parkin, Handbook of magnetism and advanced magnetic materials, John Wiley and Sons, Inc., Hoboken, New Jersey, 2007.
3 M. S. Altman, Trends in low energy electron microscopy, J. Phys: Cond. Matter, 22 (2010) 084017. DOI: 10.1088/0953-8984/22/8/084017.
4 M. S. Altman, H. Pinkvos, J. Hurst, H. Poppa, G. Marx and E. Bauer, Spin polarized low energy electron microscopy on surface magnetic structure, MRS Proceedings, 232 (1991) 125.
5 Q. Wu, R. Zydb, E. Bauer and M. S. Altman, Growth, magnetism and ferromagnetic thickness gap in Fe films on the W(111) surface, Phys, Rev. B 87 (2013) 104410.
6 G. Chen, A. Mascaraque, A. T. N'Diaye and A. K. Schmid, Room temperature skyrmion ground state stabilized through interlayer exchange coupling, Appl. Phys. Lett. 106 (2015) 242404.
7 J. E. Prieto, G Chen, A. K. Schmid and J. de la Figuera, Magnetism of epitaxial Tb films on W(110) studied by spin-polarized low-energy electron microscopy, Phys. Rev. B 94 (2016) 174445.
8 M. Suzuki, K. Ando, K. Kojima, T. Yasue, N. Akutsu, W. A. Dino, H. Kasai, E. Bauer and T. Koshikawa, Magnetic domain patterns on strong perpendicular magnetization of Co/Ni multilayers as spintronics materials: I. Dynamic observations, J. Phys.: Condens. Matter 25 (2013) 406001.
9 K. L. Man, M. S. Altman and H. Poppa, Spin polarized low energy electron microscopy investigations of magnetic transitions in Fe/Cu(100), Surf. Sci., 480 (2001) 163-172.
10 Y. Z. Wu, C. Won, A. Scholl, A. Doran, H. W. Zhao, X. F. Jin and Z. Q. Qiu, Magnetic stripe domains in coupled magnetic sandwiches, Phys. Rev. Lett. 93 (2004) 117205.
11 R. Zdyb and E. Bauer, Magnetic domain structure and spin-reorientation transition in ultrathin Fe-Co alloy films, Phys. Rev. B 67 (2003) 134420.
12 C. Klein, R. Ramchal, A. K. Schmid and M. Farle, Controlling the kinetic order of spin-reorientation transitions in Ni/Cu(100) films by tuning the substrate step structure, Phys. Rev. B 75 (2007) 193405.
13 H. F. Ding, A. K. Schmid, Dongqi Li, K. Yu. Guslienko and S. D. Bader, Magnetic bistability of Co nanodots, Phys. Rev. Lett. 94 (2005) 157202.
14 R. Zdyb, A. Pavlovska, M. Jalochowski and E. Bauer, Self-organized Fe nanostructures on W(110), Surf. Sci. 600 (2006) 1586-1991.
15 Y. R. Niu, K. L. Man, A. Pavlovska, E. Bauer and M. S. Altman, Fe on W(001) from continuous films to nanoparticles: Growth and magnetic domain structure, Phys. Rev. B 95 (2016) 064404.
16 G. Chen, J. Zhu, A. Quesada, J. Li, A. T. N'Diaye, Y. Huo, T. P. Ma, Y. Chen, H. Y. Kwon, C. Won, Z. Q. Qiu, A. K. Schmid and Y. Z. Wu, Novel chiral magnetic DW structure in Fe/Ni/Cu(001) films, Phys. Rev. Lett. 110 (2013) 177204.
17 G. Chen, T. Ma, A. T. N'Diaye, H. Kwon, C. Won, Y. Wu and A. K. Schmid, Tailoring the chirality of magnetic DWs by interface engineering. Nat. Commun. 4 (2013) 2671.

18 G. Chen, S. P. Kang, C. Ophus, A. T. N'Diaye, H. Y. Kwon, R. T. Qiu, C. Won, K. Liu and Y. Wu, A. K. Schmid, Out-of-plane chiral DW spin structures in ultrathin in-plane magnets. Nat. Commun. 8 (2017) 15302.
19 Hongxin Yang, Gong Chen, Alexandre AC Cotta, Alpha T N'Diaye, Sergey A Nikolaev, Edmar A Soares, Waldemar AA Macedo, Kai Liu, Andreas K Schmid, Albert Fert, Mairbek Chshiev, Significant Dzyaloshinskii–Moriya interaction at graphene–ferromagnet interfaces due to the Rashba effect. Nat. Mater. 17 (2018) 605.
20 M. S. Altman, Trends in low energy electron microscopy, J. Phys.: Condens. Matter, 22 (2010) 084017.
21 M. S. Altman, W. F. Chung, Z. Q. He, H. C. Poon and S. Y. Tong, Quantum size effect in low energy electron diffraction of thin films, Appl. Surf. Sci., 169-170 (2001) 82-87.
22 R. Zdyb and E. Bauer, Spin-resolved unoccupied electronic band structure from quantum size oscillations in the reflectivity of slow electrons from ultrathin ferromagnetic crystals, Phys. Rev. Lett. 88 (2002) 166403.
23 Y. Z. Wu, A. K. Schmid, M. S. Altman, X. F. Jin and Z. Q. Qiu, Spin-dependent Fabry-Pérot interference from a Cu thin film grown on fcc Co(001), Phys. Rev. Lett., 94 (2005) 027201.
24 J. Graf, C. Jozwiak, A. K. Schmid, Z. Hussain and A. Lanzara, Mapping the spin-dependent electron reflectivity of Fe and Co ferromagnetic thin films, Phys. Rev. B 71 (2005) 144429.
25 Y. Z. Wu, A. K. Schmid and Z. Q. Qiu, Spin-dependent quantum interference from epitaxial MgO thin films on Fe(001), Phys. Rev. Lett., 97 (2006) 217205.
26 C. Hanneken, F. Otte, A. Kubetzka, B. Dupé, N. Romming, K. von Bergmann, R. Wiesendanger and S. Heinze, Electrical detection of magnetic skyrmions by tunneling non-collinear magnetoresistance, Nat. Nanotechnol. 10 (2015) 1039-1042.
27 H. Fritzsche, J. Kohlhepp and U. Gradmann, Epitaxial strain and magnetic anisotropy in ultrathin Co films on W(110), Phys. Rev. Lett. 51 (1995) 15933-15941.
28 A. Hubert and R. Schafer, Magnetic domains: the analysis of magnetic microstructures. Springer-Verlag Berlin Heidelberg (1998), DOI: 10.1007/978-3-540-85054-0.
29 P. Krams, F. Lauks, R. L. Stamps, B. Hillebrands, and G. Güntherodt, Magnetic anisotropies of ultrathin Co(001) films on Cu(001), Phys. Rev. Lett. 69 (1992) 3674.
30 R. K. Kawakami, M. O. Bowen, Hyuk J. Choi, Ernesto J. Escorcia-Aparicio and Z. Q. Qiu, Effect of atomic steps on the magnetic anisotropy in vicinal Co/Cu(001), Phys. Rev. B 58 (1998) R5924.
31 R. Schäfer, C. Hamann, J. McCord, L. Schultz and V. Kamberský, The magneto-optical gradient effect in an exchange-biased thin film: experimental evidence for classical diffraction theory, New Journal of Physics 12 (2010) 053006.
32 W. Kuch, R. Schäfer, P. Fischer and F. U. Hillebrecht, Magnetic microscopy of layered structures, Springer-Verlag Berlin Heidelberg (2015) DOI: 10.1007/978-3-662-44532-7.
33 R. Schäfer and A. Hubert, A new magnetooptic effect related to non−uniform magnetization on the surface of a ferromagnet, Phys. Stat. Sol. A 118 (1990) 271-288.
34 V. Kamberský. On magnetooptical effects caused by the gradient of magnetization. Phys. Stat. Sol. A 123 (1991) K71.
35 V. Kamberský. A Further Contribution to the Magneto-Optical Effects Caused By a

Gradient of Magnetization. Phys. Stat. Sol. A 125 (1991) K117.
36 N. Rougemaille, F. El Gabaly, R. Stumpf, A. K. Schmid, K. Thürmer, N. C. Bartelt, and J. de la Figuera, Labyrinthine Island Growth during Pd/Ru(0001) Heteroepitaxy. Phys. Rev. Lett. 99 (2007) 106101.

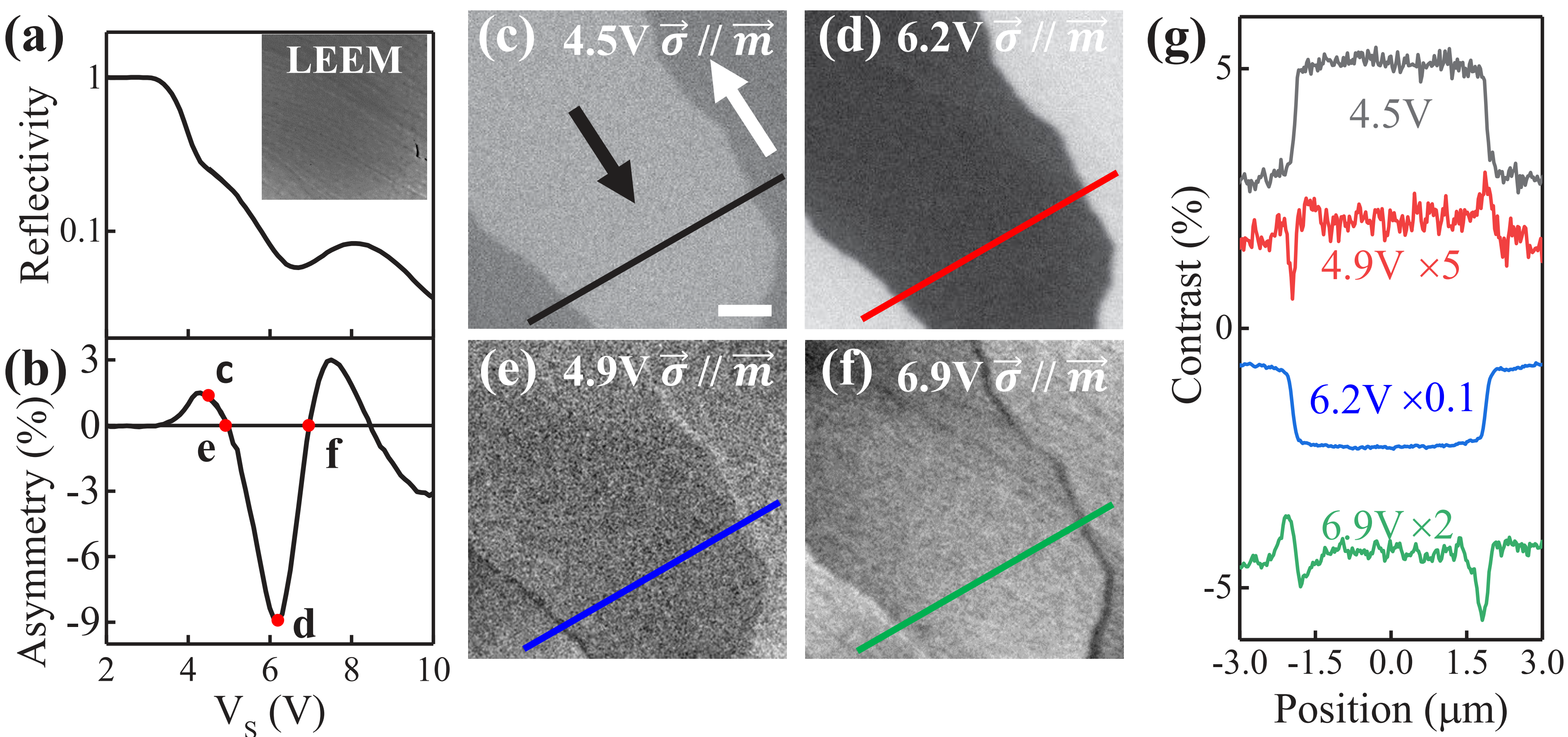
(a)
LEEM
Reflectivity
1
0.1
(b)
Asymmetry (%)
3
0
-3
-6
-9
c
e
f
d
2
4
6
8
10
V_S (V)
(c) 4.5V $\vec{\sigma}$ // $\vec{m}$
(d) 6.2V $\vec{\sigma}$ // $\vec{m}$
(e) 4.9V $\vec{\sigma}$ // $\vec{m}$
(f) 6.9V $\vec{\sigma}$ // $\vec{m}$
(g)
Contrast (%)
5
0
-5
4.5V
4.9V ×5
6.2V ×0.1
6.9V ×2
-3.0
-1.5
0.0
1.5
3.0
Position (μm)

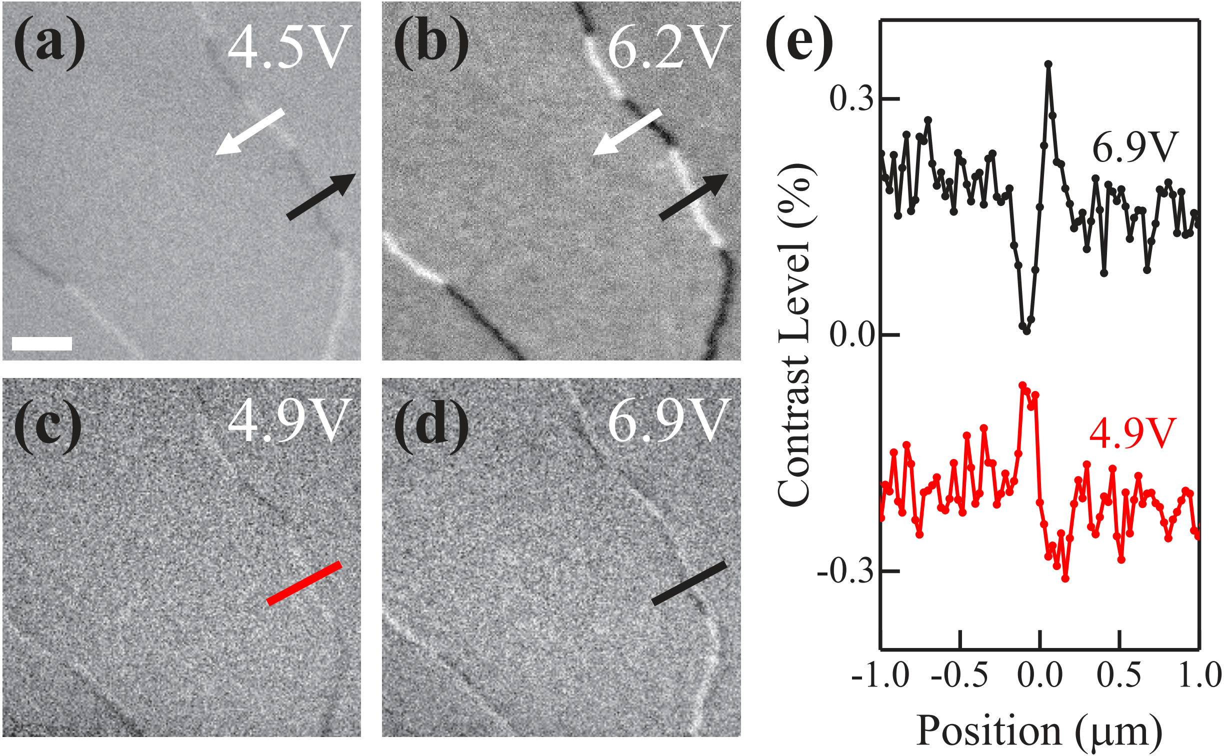

(a)
4.5V
(b)
6.2V
(c)
4.9V
(d)
6.9V
(e)
6.9V
4.9V
0.3
0.0
-0.3
Contrast Level (%)
-1.0
-0.5
0.0
0.5
1.0
Position (μm)

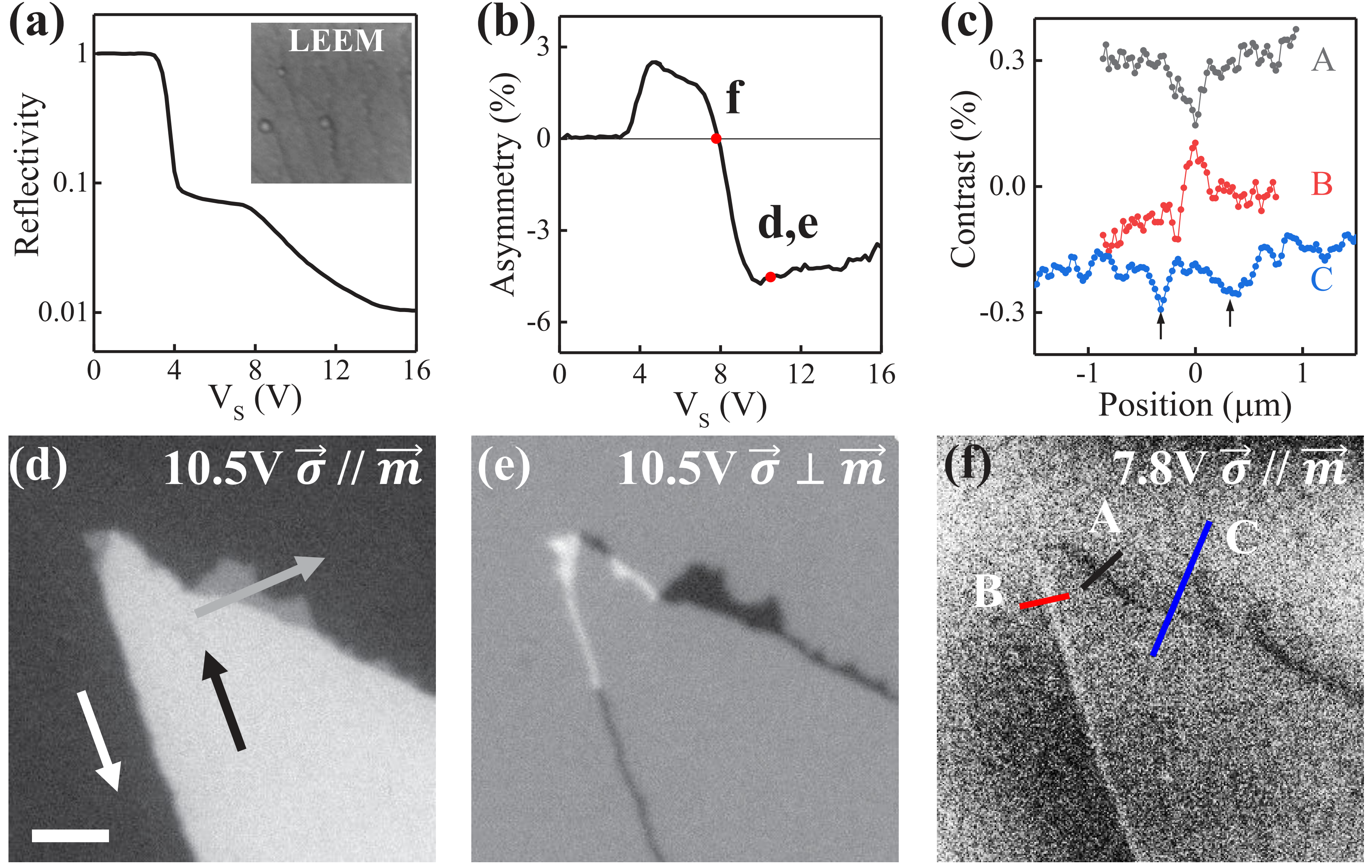

(a)
LEEM
Reflectivity
1
0.1
0.01
0
4
8
12
16
V_S (V)
(b)
Asymmetry (%)
3
0
-3
-6
f
d,e
0
4
8
12
16
V_S (V)
(c)
Contrast (%)
0.3
0.0
-0.3
A
B
C
-1
0
1
Position (μm)
(d)
10.5V σ // m
(e)
10.5V σ ⊥ m
(f)
7.8V σ // m
A
B
C

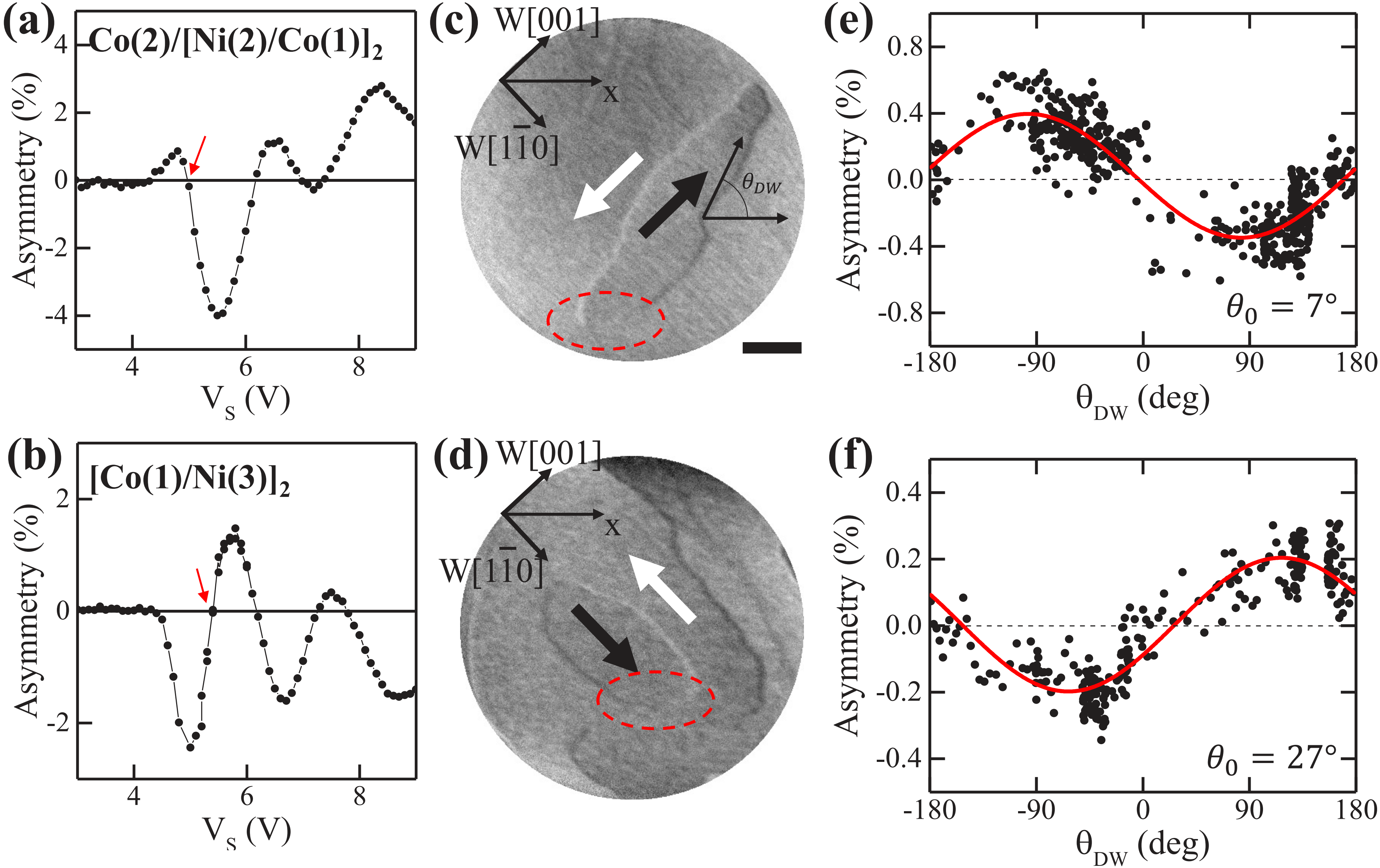

(a)
Co(2)/[Ni(2)/Co(1)]$_2$
Asymmetry (%)
V_S (V)
(b)
[Co(1)/Ni(3)]$_2$
Asymmetry (%)
V_S (V)
(c)
W[001]
x
W[1$\bar{1}$0]
θ_{DW}
(d)
W[001]
x
W[1$\bar{1}$0]
(e)
Asymmetry (%)
θ_0 = 7°
θ_{DW} (deg)
(f)
Asymmetry (%)
θ_0 = 27°
θ_{DW} (deg)

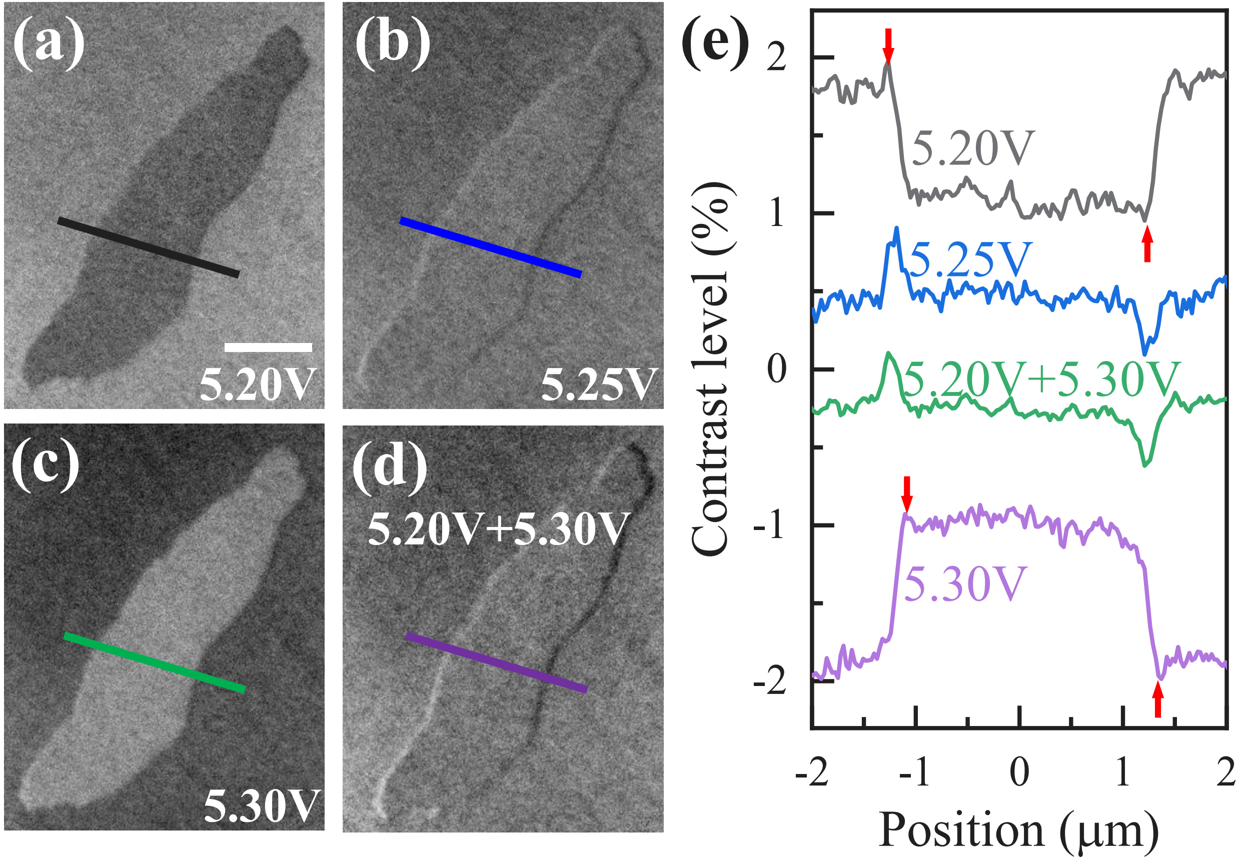
(a)
5.20V
(b)
5.25V
(c)
5.30V
(d)
5.20V+5.30V
(e)
5.20V
5.25V
5.20V+5.30V
5.30V
Contrast level (%)
Position (μm)
2
1
0
-1
-2
-2
-1
0
1
2

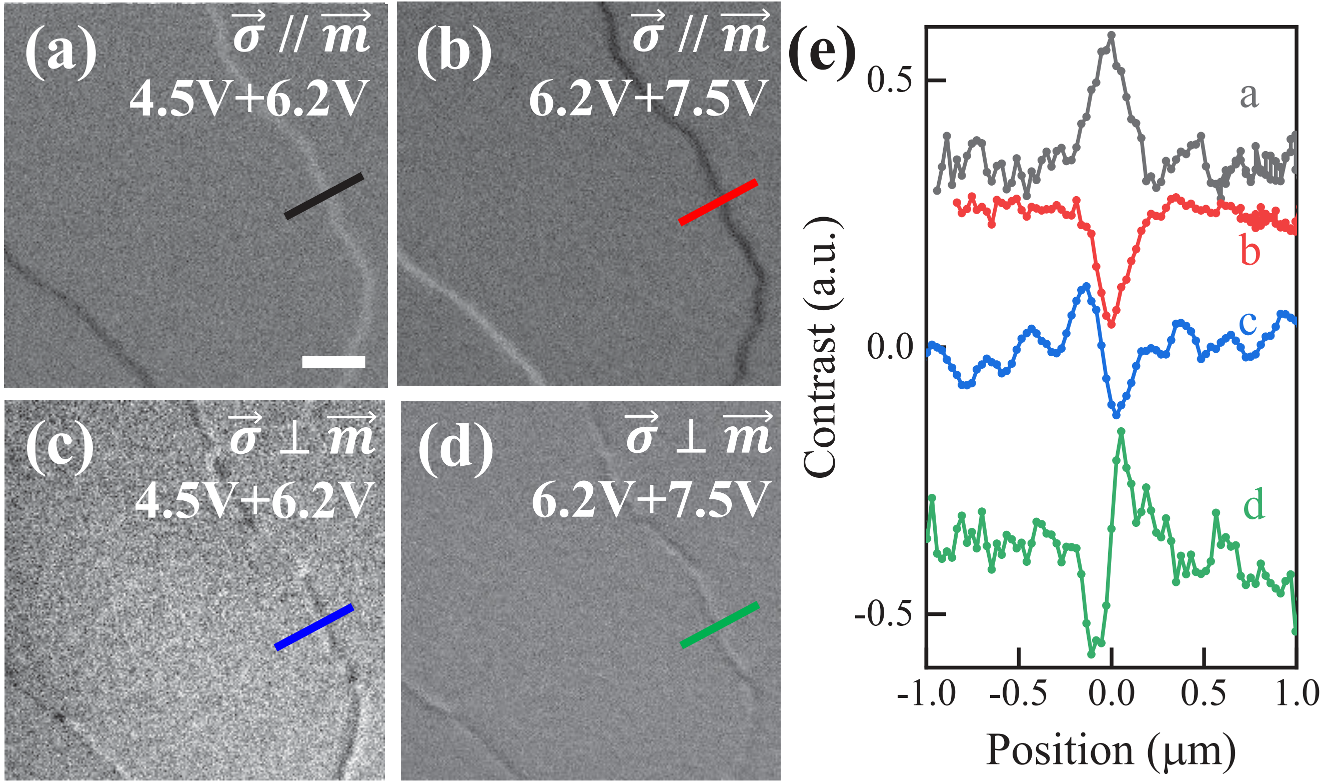

(a)
$\vec{\sigma} // \vec{m}$
4.5V+6.2V
(b)
$\vec{\sigma} // \vec{m}$
6.2V+7.5V
(c)
$\vec{\sigma} \perp \vec{m}$
4.5V+6.2V
(d)
$\vec{\sigma} \perp \vec{m}$
6.2V+7.5V
(e)
Contrast (a.u.)
0.5
0.0
-0.5
a
b
c
d
-1.0
-0.5
0.0
0.5
1.0
Position (μm)

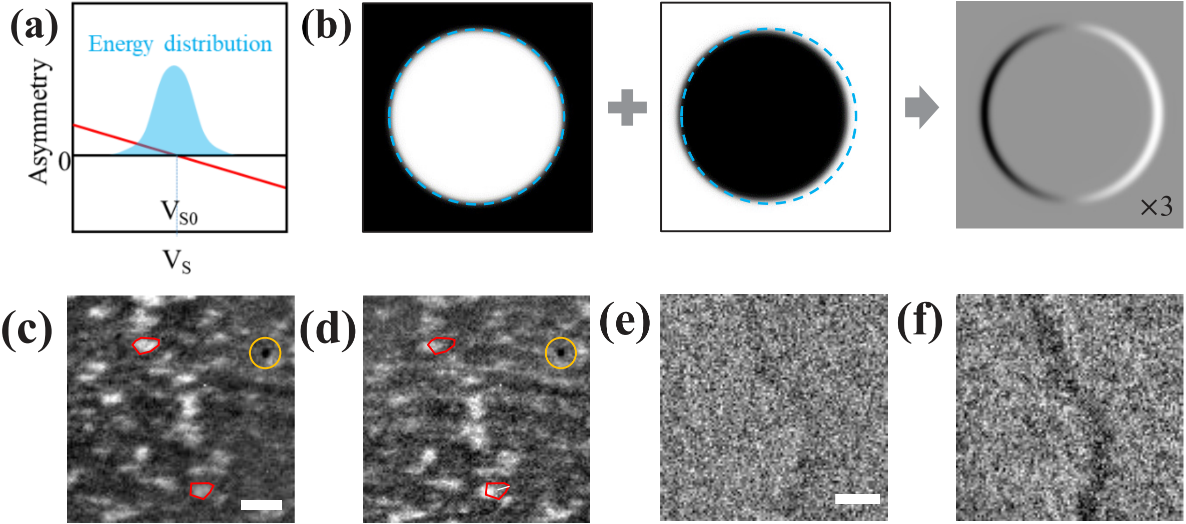
(a)
Energy distribution
Asymmetry
0
V_{S0}
V_S
(b)
×3
(c)
(d)
(e)
(f)